

Neuron, Volume 76

Supplemental Information

**A Continuous Semantic Space Describes
the Representation of Thousands of Object
and Action Categories across the Human Brain**

Alexander G. Huth, Shinji Nishimoto, An T. Vu, and Jack L. Gallant





Movie Clip	Labels	Movie Clip	Labels
	<p> butte.n.01 desert.n.01 sky.n.01 cloud.n.01 brush.n.01 </p>		<p> city.n.01 expressway.n.01 skyscraper.n.01 traffic.n.01 sky.n.01 </p>
	<p> woman.n.01 talk.v.02 gesticulate.v.01 book.n.01 </p>		<p> bison.n.01 walk.v.01 grass.n.01 stream.n.01 </p>
	<p> hammerhead.n.01 swim.v.01 water.n.01 </p>		<p> woman.n.01 man.n.01 talk.v.02 </p>

Figure S1 (related to Figure 1). Example stimuli with category labels. Representative frames from six movie clips that were used as stimuli in this experiment, along with the labels that were assigned to those clips. The WordNet lexicon (Miller, 1995) was used to label salient objects and actions in each second of the movies. Each WordNet label (e.g. *bison.n.01*) has a name (*bison*), a part-of-speech (*n* for noun or *v* for verb), and a number (*01*, indicating the first meaning of bison).

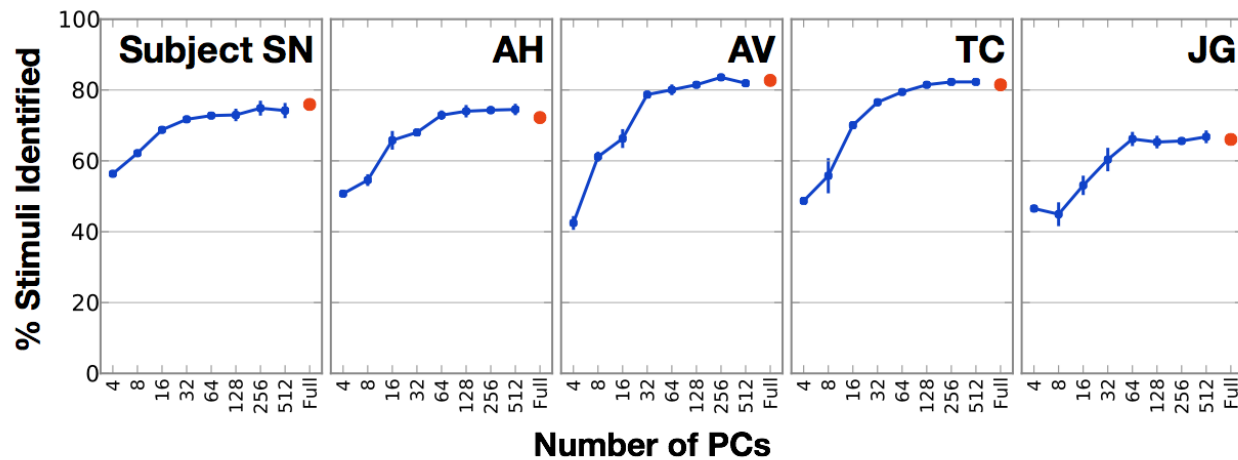


Figure S2 (related to Figure 3). Stimulus identification accuracy using different numbers of group PCs. We used an identification analysis (Kay et al., 2008; Nishimoto et al., 2011) to quantify the amount of information retained in the semantic space defined by the group PCs. Identification accuracy measures how well a model can associate BOLD responses observed across a voxel population with the stimuli that evoked them (see Experimental Procedures for details). Here we show the identification accuracy for each subject in a separate panel. Identification accuracy for the full category model is shown as a red marker. Identification accuracy for models based on different numbers of group PCs (4 – 512) are shown as blue markers. The voxel set used to construct the group PC space was bootstrapped 10 times, and error bars here show the minimum and maximum identification accuracy over the 10 bootstrap samples, while the markers show the average identification accuracy across the 10 samples. The full category model can correctly identify an average of 76% of stimuli across subjects (chance is 1.9%), while the model based on the 4-PC group space can correctly identify 49% of the stimuli, roughly two thirds as many as the full model. These results show that the 4-PC group space does not capture all of the stimulus-related information present in the full category model, indicating that the true semantic space likely has many more than four dimensions. Further experiments will be required to significantly resolve the other semantic dimensions. Note that models based on 64 or more group PCs have approximately the same identification accuracy as the full category model.

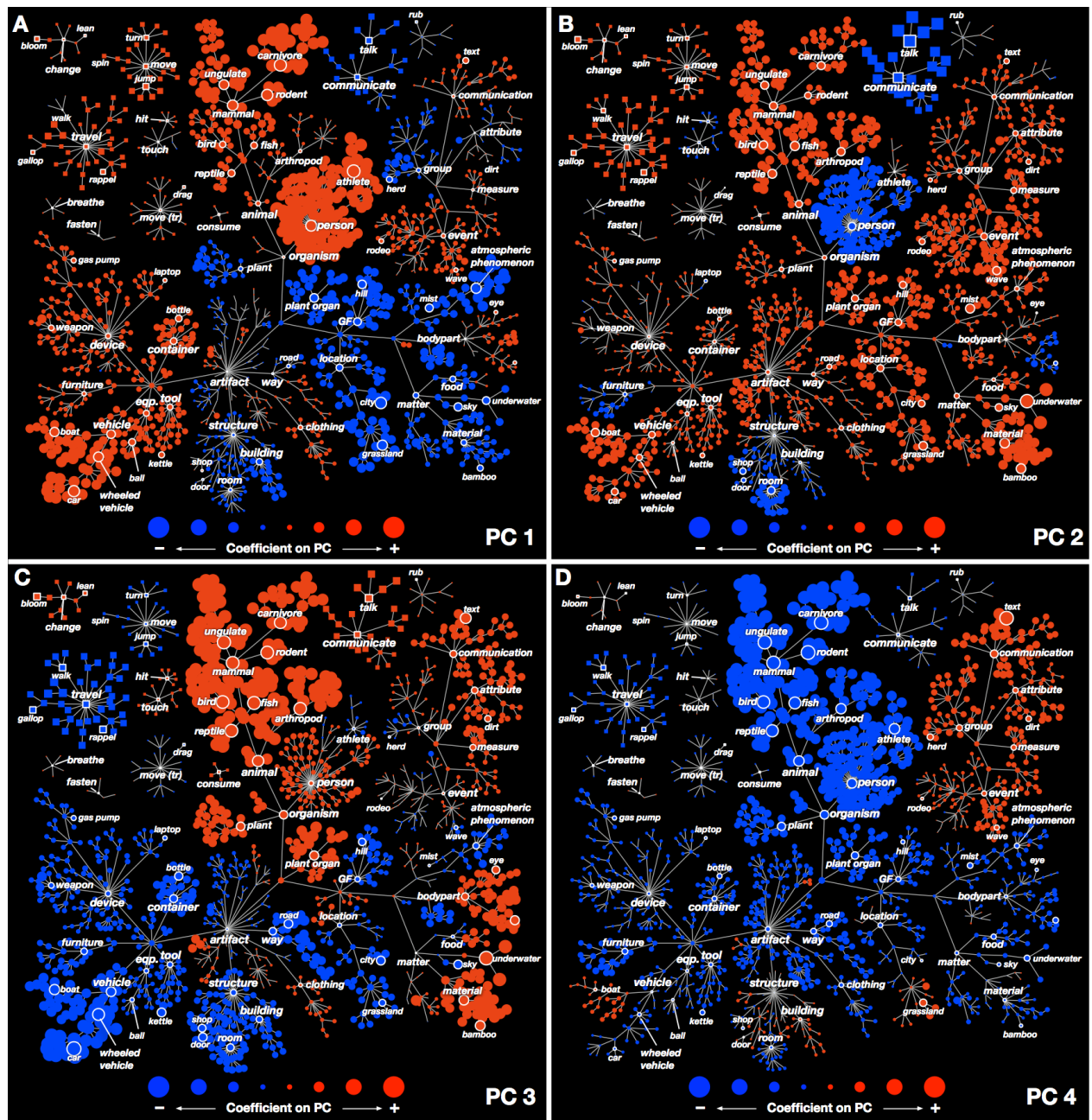


Figure S3 (related to Figure 4). Coefficients of the 1st-4th group semantic PCs. Each panel shows all 1705 categories, organized according to the graphical structure of WordNet. Each marker represents a single noun (circle) or verb (square). Red markers indicate positive coefficients and blue negative. The size of each marker indicates the magnitude of its coefficient on the PC. (A) The first PC distinguishes between categories with high stimulus energy (e.g. moving objects like *person* and *vehicle*) and low stimulus energy (e.g. stationary objects like *sky* and *city*). (B) The second PC distinguishes between categories involved in social interaction (e.g., *people*, communication verbs, *indoor spaces*, *body parts*, and *furniture*) and those involved in outdoor activities and actions (e.g., *animals*, *vehicles*, *outdoor events*, *geological formations*, movement verbs, and *landscapes*). (C) The third PC distinguishes between categories associated with nature (e.g., *animals*, *plants*, *body parts*, and *materials*) and categories associated with civilization (e.g., *vehicles*, *roads*, and *indoor spaces*). (D) The fourth PC is difficult to interpret, but roughly distinguishes between living categories (e.g., *animals*, *people*, and *plants*) and most other categories (particularly *text*).

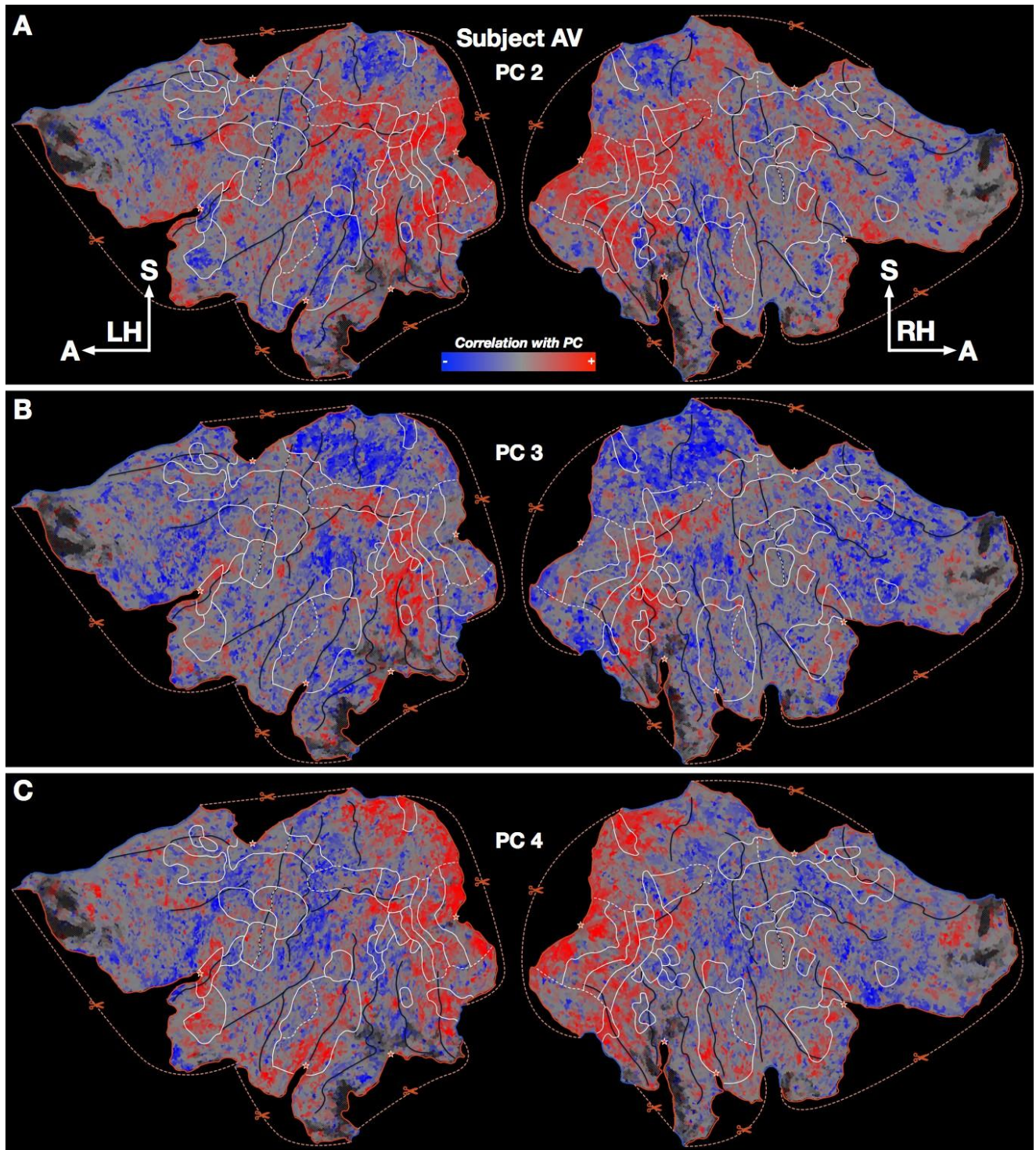


Figure S4 (related to Figure 7). Cortical flat maps with individual PC projections. Similar to Figure 7 in the main text, this figure shows the second, third, and fourth group semantic PCs projected on the cortical flat map constructed specially for subject AV. (A) Each location on the map represents a single voxel in subject AV. The color reflects the projection of the voxel category model weights on the second PC (shown in Figure S3B). Voxels that are positively correlated with the second PC appear red, while negatively correlated voxels appear blue. Voxels orthogonal to the second PC appear gray. (B) Same, for third PC. (C) Same, for fourth PC.

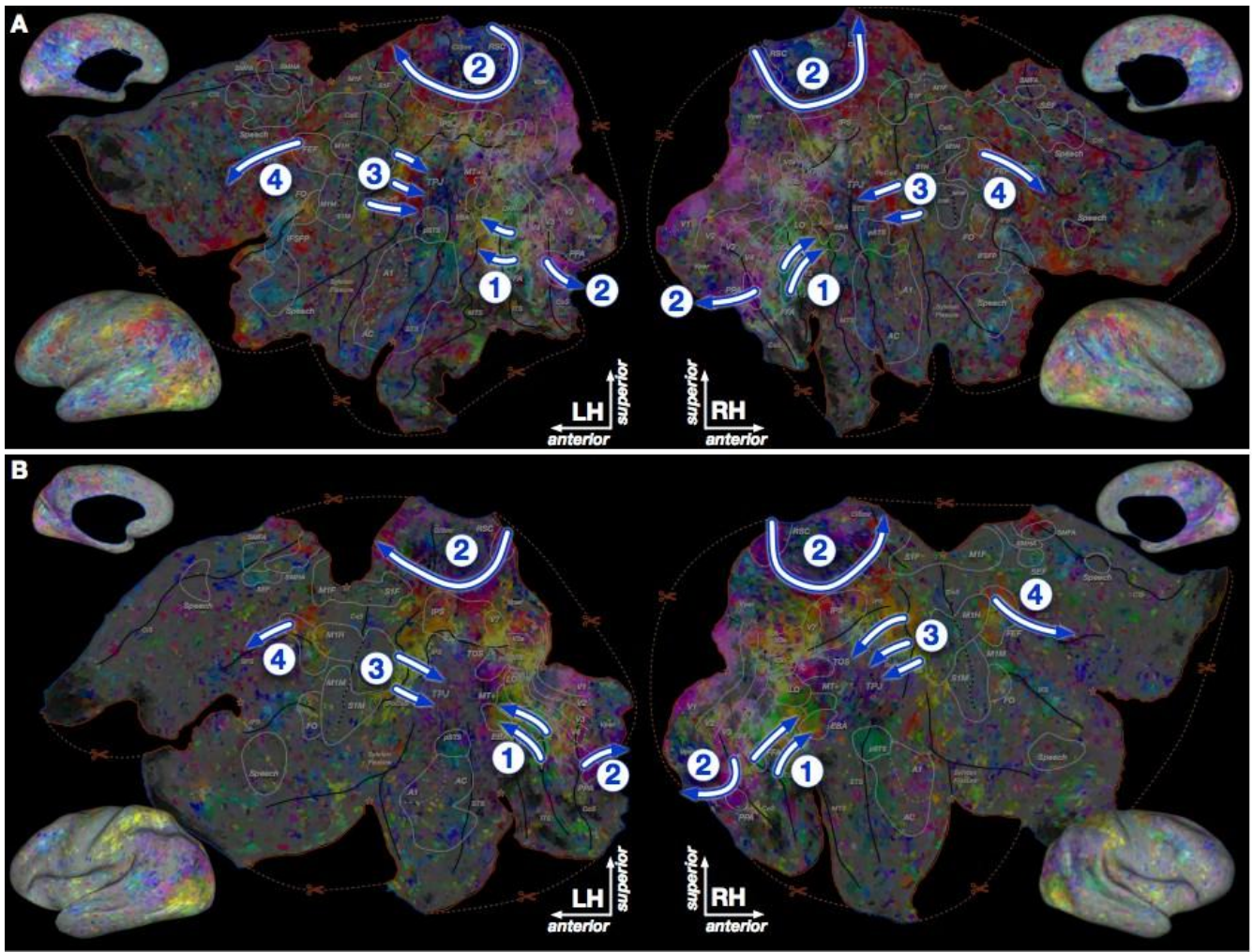


Figure S6 (related to Figure 7). Schematic of semantic gradients. This figure is similar to Figure 7 in the main text, but shows schematically the semantic gradients that appear consistently across subjects. These gradients are described in detail in the main text. **(A)** The cortical flat map constructed for subject AV. Semantic gradients are indicated by blue and white arrows and numbered. **Gradient 1** starts in the posterior inferior temporal sulcus (ITS), which is selective for humans (green and blue-green), continues through a region of animal selectivity (yellow), and ends at the posterior middle temporal sulcus (MTS), which is selective for human actions, athletes, and outdoor spaces (red and green-red). **Gradient 2** starts in a region of the collateral sulcus that is selective for vehicles and landscapes (pink and purple), continues superiorly along the medial wall to retrosplenial cortex (RSC), which is selective for buildings and landscapes (blue-indigo and purple), then continues anteriorly along the superior bank of the intraparietal sulcus (IPS), which is selective for geography and human actions (red-purple and red). Note that this gradient crosses one of the relaxation cuts made to the cortical surface, and so appears discontinuous. **Gradient 3** starts in the inferior postcentral sulcus (PoCeS), which is animal selective (yellow and yellow-green), and ends in the anterior part of the temporoparietal junction (TPJ), which is landscape selective (purple). **Gradient 4** starts in the posterior superior frontal sulcus (SFS), which is selective for human actions (red), and ends in the anterior SFS, which is selective for landscapes (purple). **(B)** The cortical flat map constructed for subject TC with semantic gradients.

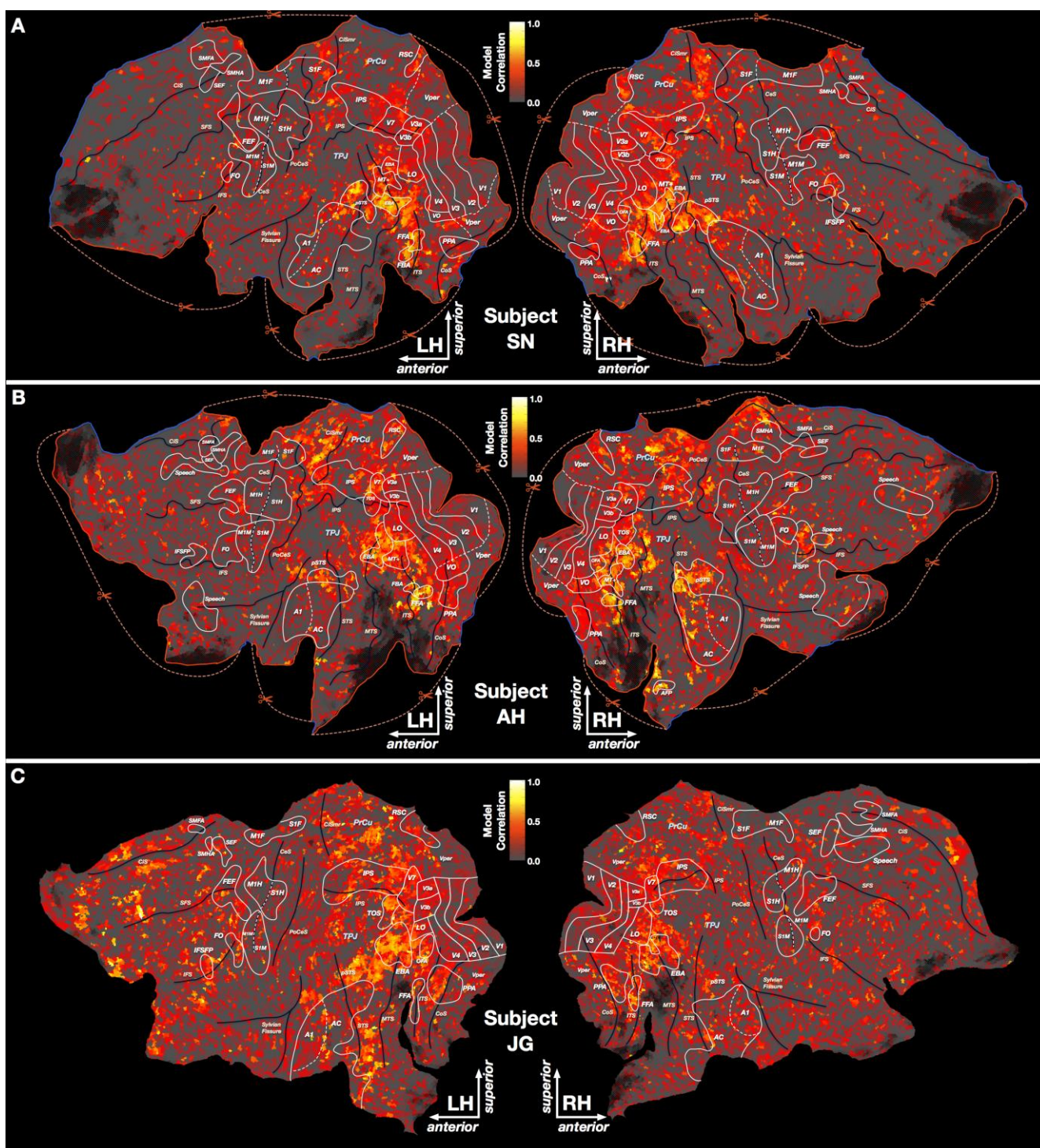


Figure S7 (related to Figure 9). Model prediction performance across the cortical surface for subjects SN, AH, and JG. To determine how much response variance for each voxel is explained by the category model, prediction performance was assessed using the validation data. (A) Each location on these maps represents a single voxel in subject SN. Well predicted voxels appear yellow or white, poorly predicted voxels appear gray. Borders and notations on the graph are as described in the earlier Figures. The best predictions are found in occipitotemporal cortex, the posterior superior temporal sulcus, medial parietal cortex, and inferior frontal cortex. (B) Model performance for subject AH. (C) Model performance for subject JG.

Table S1 (related to Figure 7). Abbreviations, localizers, and references for known functional areas

<i>Name</i>	<i>Anatomical Location</i>	<i>Localizer</i>	<i>References</i>
FFA (fusiform face area)	Posterior fusiform gyrus	Faces – objects contrast	Kanwisher et al., 1997; McCarthy et al., 1997
OFA (occipital face area)	Just anterior to V4v/VO	Faces – objects contrast	Halgren et al., 1999; Kanwisher et al., 1997
IFSFP (inferior frontal sulcus face patch)	IFS anterior to precentral sulcus	Faces – objects contrast	Avidan et al., 2005; Tsao et al., 2008
ATFP (anterior temporal face patch)	Temporal pole	Faces – objects contrast	Rajimehr et al., 2009
EBA (extrastriate body area)	Anterior to MT+ on the medial temporal gyrus	Human bodies – objects contrast	Downing et al., 2001
FBA (fusiform body area)	Fusiform sulcus/gyrus anterior to FFA	Human bodies – objects contrast	Peelen & Downing, 2005; Schwarzlose et al., 2005
PPA (parahippocampal place area)	Collateral fissure	Scenes – objects contrast	Epstein & Kanwisher, 1998
TOS (transverse occipital sulcus)	Just inferior to/overlapping with V7	Scenes – objects contrast	Hasson et al., 2003; K. Nakamura et al., 2000
RSC (retrosplenial cortex)	Medial wall just superior to PPA	Scenes – objects contrast	Aguirre, Zarahn, & D'esposito, 1998
FEF (frontal eye fields)	Precentral sulcus and superior frontal sulcus	Self generated saccades – fixation contrast	Paus, 1996
FO (frontal operculum)	Inferior portion of precentral sulcus	Self generated saccades – fixation contrast	Corbetta et al., 1998
SEF (supplementary eye fields)	Dorsal-medial frontal cortex	Self generated saccades – fixation contrast	Grosbras et al., 1999
Vper (visual periphery, including V1-V4)	Surrounding mapped retinotopic visual cortex	Self generated saccades – fixation contrast	
MT+ (middle temporal)	Posterior inferior temporal sulcus	Coherent – scrambled motion contrast	Tootell et al., 1995
pSTS (posterior superior temporal sulcus)	As it sounds	High auditory and visual repeatability	
A1 (primary auditory cortex)	Heschl's gyri	Auditory repeatability and anatomical location	
AC (auditory cortex)	Superior temporal gyrus	Auditory repeatability	
S1F/M1F (primary somatosensory and motor cortex, foot)	Superior-medial central sulcus	Foot motion – rest contrast, S1F and M1F split at fundus of central sulcus	Penfield & Boldrey, 1937
S1H/M1H (primary somatosensory and motor cortex, hand)	Central sulcus	Hand motion – rest contrast, S1H and M1H split at fundus of central sulcus	Penfield & Boldrey, 1937
S1M/M1M (primary somatosensory and motor cortex, mouth)	Inferior central sulcus	Mouth motion – rest contrast, S1M and M1M split at fundus of central sulcus	Penfield & Boldrey, 1937

<i>Name</i>	<i>Anatomical Location</i>	<i>Localizer</i>	<i>References</i>
SMHA (supplementary motor hand area)	Middle cingulate gyrus	Hand motion – rest contrast	Fried et al., 1991
SMFA (supplementary motor foot area)	Middle cingulate gyrus/sulcus	Foot motion – rest contrast	Fried et al., 1991
IPS (intraparietal sulcus)	Lateral parietal cortex	Retinotopy	
V1-V4, V3A, V3B	Occipital cortex	Retinotopy	Hansen et al., 2007
LO (lat. occipital complex)	Anterior to V4	Retinotopy	Hansen et al., 2007
VO	Inferior to V4v	Retinotopy	Brewer et al., 2005
V7	Anterior to V3A/V3B	Retinotopy	Hansen et al., 2007

Table S2 (related to Figure 7). Abbreviations for anatomical features

<i>Abbreviation</i>	<i>Full Name</i>
CoS	Collateral sulcus
ITS	Inferior temporal sulcus
MTS	Middle temporal sulcus
STS	Superior temporal sulcus
IPS	Intraparietal sulcus
CiSmr	Marginal ramus of the cingulate sulcus
PoCeS	Postcentral sulcus
CeS	Central sulcus
IFS	Inferior frontal sulcus
SFS	Superior frontal sulcus
CiS	Cingulate sulcus
PrCu	Precuneus
TPJ	Temporoparietal junction

Table S3 (related to Figure 9). Category model performance within known functional areas

<i>Area</i>	<i>Hemi.</i>	<i>N</i>	<i>Avg. Corr.</i>	<i>Signif. / Total Voxels</i>
A1	L	4	0.088	14 / 152
	R	4	0.100	20 / 148
AC (incl. A1)	L	5	0.152	124 / 633
	R	5	0.166	139 / 572
ATFP	L	0	–	–
	R	1	0.298	3 / 8
EBA	L	5	0.449	146 / 172
	R	5	0.430	123 / 158
FBA	L	2	0.367	4 / 7
	R	1	0.525	8 / 10
FEF	L	5	0.164	65 / 216
	R	5	0.165	47 / 167
FFA	L	5	0.387	39 / 61
	R	5	0.441	58 / 72
FO	L	5	0.143	24 / 108
	R	5	0.191	24 / 74
IFSFP	L	3	0.254	21 / 53
	R	3	0.230	37 / 89
IPS	L	5	0.219	163 / 364
	R	5	0.224	147 / 316
LO	L	5	0.286	87 / 117
	R	5	0.311	120 / 165
MT+	L	4	0.378	68 / 82
	R	4	0.429	53 / 59
OFA	L	3	0.322	15 / 24
	R	3	0.312	19 / 26
PPA	L	5	0.263	70 / 123
	R	5	0.298	46 / 68
RSC	L	5	0.239	32 / 75
	R	5	0.244	46 / 107
SEF	L	4	0.110	3 / 29
	R	4	0.110	3 / 34
TOS	L	3	0.327	32 / 58
	R	4	0.322	53 / 75
V1	L	5	0.109	60 / 248
	R	5	0.111	75 / 279
V2	L	5	0.115	92 / 294
	R	5	0.125	111 / 332
V3	L	5	0.125	82 / 243
	R	5	0.147	113 / 281
V3A	L	5	0.205	40 / 69
	R	5	0.236	47 / 74
V3B	L	5	0.208	37 / 67
	R	5	0.236	50 / 77

<i>Area</i>	<i>Hemi.</i>	<i>N</i>	<i>Avg. Corr.</i>	<i>Signif. / Total Voxels</i>
V4	L	5	0.160	85 / 197
	R	5	0.184	101 / 211
V7	L	5	0.292	79 / 110
	R	5	0.266	95 / 137
VO	L	2	0.204	16 / 26
	R	2	0.237	27 / 35
Foot (S1/M1)	L	5	0.102	30 / 220
	R	5	0.083	21 / 209
Hand (S1/M1)	L	5	0.081	29 / 365
	R	5	0.091	25 / 290
Mouth (S1/M1)	L	5	0.093	31 / 280
	R	5	0.091	22 / 229
pSTS	L	4	0.348	63 / 107
	R	4	0.385	95 / 137

Prediction performance of the 1705-category model within known functional areas. For each area in each hemisphere, this table shows the number of subjects in which the area was identified (N), the average correlation coefficient within the area (corrected to account for noise in the validation dataset), the average number of voxels whose activity was predicted significantly ($p < 0.05$ uncorrected), and the average total number of voxels within the area (each voxel is 20.7mm^3 in volume).

Supplemental Experimental Procedures

Functional localizers

Retinotopic localizer. Retinotopic mapping data were collected in four 9-minute scans. Two scans used clockwise and counterclockwise rotating polar wedges, and two used expanding and contracting rings.

Motor localizer. Motor localizer data were collected during one 10-minute scan. The subject was cued to perform six different motor tasks in a random order in 20-second blocks. For the hand, mouth, foot, speech, and rest blocks the stimulus was simply a word at the center of the screen (e.g. "Hand"). For the saccade block the subject was shown a pattern of saccade targets.

For the "Hand" cue the subject was instructed to make small finger-drumming movements with both hands for as long as the cue remained on the screen. Similarly for the "Foot" cue the subject was instructed to make small toe movements for the duration of the cue. For the "Mouth" cue the subject was instructed to make small mouth movements approximating the nonsense syllable *balabalabala* for the duration of the cue--this requires movement of the lips, tongue, and jaw. For the "Speak" cue the subject was instructed to continuously subvocalize self-generated sentences for the duration of the cue. For the saccade condition the written cue was replaced with a fixed pattern of twelve saccade targets, and the subject was instructed to make frequent saccades between the targets.

Area MT+ localizer. Area MT+ localizer data were collected in four 90-second scans consisting of alternating 16-second blocks of continuous and temporally scrambled natural movies.

Visual category localizers. Visual category localizer data were collected in six 4.5-minute scans consisting of 16 blocks, each 16 seconds long. During each block, 20 images of either places, faces, human body parts, non-human animals, household objects, or spatially scrambled household objects were displayed. Each image was displayed for 300 ms followed by a 500 ms blank. Occasionally the same image was displayed twice in a row, in which case the subject was asked to respond with a button press.

Auditory localizer. Auditory cortex localizer data were collected in one 10 minute scan. The subject listened to 10 repeats of a 1-minute auditory stimulus, which consisted of 20-second segments of music, speech, and natural sounds. To determine whether a voxel was responsive to auditory stimuli, the repeatability of the voxel response across the 10 stimulus repeats was calculated using an *F*-statistic.

RGB colormap construction

Principal components analysis (PCA) produces a low-dimensional orthogonal space. While each dimension is not necessarily interpretable on its own, the space as a whole is highly interpretable (see Fig. 5). In order to visualize projections of voxel models and categories in a three-dimensional space we constructed a trivariate colormap. In this colormap each location in the 3-D unit cube is mapped to a unique color. We used this scheme to visualize both category coefficients and model projections into the PC space. However, we do not expect these data to map uniformly onto a cube. Instead, the distribution of model projections tends to be spherical. Mapping spherical data onto the RGB cube is inefficient, as the corners of the color space (where the strongest colors reside) are underutilized. Thus we devised a modified RGB colormap that could efficiently map spherical data onto unique RGB values.

Our modified RGB map can be thought of as a 3-dimensional sphere in which each point represents a

unique RGB value. This sphere is derived from the original RGB cube (a unit cube centered at the origin) by the following procedure: the coordinates of each point within the cube are first normalized by their L-infinity norm (the maximum value of the three coordinates) and then multiplied by their L-2, or Euclidean norm. This procedure maps the unit cube onto a unit sphere.

Voxel-wise model fitting and testing

L2-penalized linear least square regression (also known as ridge regression) was used to find weights on the feature channels that best predicted responses on the model estimation data, which consisted of 7200 seconds of stimuli and responses. The following procedure was repeated 15 times: we fit the model using a range of regularization coefficients on all but a randomly selected 500 seconds of model estimation data (for a total of 6700 seconds of training data). Using the weights found for each regularization coefficient we predicted the responses to the held-out 500 seconds of data and computed the correlation between actual and predicted responses separately for each voxel. Once this was done 15 times, the test correlations for each voxel and regularization coefficient were averaged across the 15 repetitions. The best regularization coefficient was then selected for each voxel.

Finally, we used all 7200 seconds of training data and the selected regularization coefficient for each voxel to fit the model. To obtain a single weight for each category and each voxel, the weights for the three delays were averaged. The resulting weights were used in all subsequent analyses.

To determine model performance we generated predictions for the 540 seconds (270 samples) of model validation data that were not used for model estimation. We then found the correlation between predicted and mean response for each voxel across the ten repetitions of the validation stimuli. To test whether a voxel was predicted significantly above chance level we used a bootstrap procedure. The 270 time points in the validation data were resampled with replacement 10,000 times and the correlation between resampled predicted and resampled actual responses was computed for each sample. The p -value of the correlation was computed as the fraction of samples for which the correlation was less than zero; under the null hypothesis of no correlation this would yield $p=0.5$. The voxels shown in Figure 2 have very high correlations (0.530 and 0.659) and p -values too small to probe using this bootstrap method. To assign p -values to these correlations we used an exact formula to compute the p -value of the correlation between two Gaussian random variables.

While the correlation between predicted response and actual mean response is an appropriate metric for assessing significance, it is biased downward due to noise in the validation data (David & Gallant, 2005; Hsu et al., 2004; Sahani & Linden, 2003). Because the actual mean response is calculated using a finite number of repetitions (in this case 10) it contains residual noise in addition to signal. This noise level is likely to vary across voxels due to vascularization and magnetic field inhomogeneity. We accounted for noise in the validation data using the method developed in Hsu et al., 2004, in which the raw correlation is divided by the expected maximum possible model correlation (called the *noise ceiling*) for each voxel. For very noisy voxels, however, this method led to divergent correlation estimates. To correct this issue we limited voxel noise ceilings to be above some value k . For $k=1$, the estimated actual correlation is the observed correlation between response and prediction, and for $k=0$ the estimated actual correlation is the original divergent estimate. We set k to 0.10, which is the $p<0.05$ significance threshold for the correlation of two gaussian variables of length 270.

Significance testing of principal components

If there is no structured semantic space underlying the true model weights (i.e. the weights for each voxel are independent from the other voxels) then the PCs of the estimated model weights will be identical to the PCs of the stimulus matrix. This bias in the estimated weight PCs is due to the regularized regression procedure, which trades a small increase in bias for a large decrease in error (Hoerl & Kennard, 1970). Thus in order to appropriately evaluate statistical significance of the estimated model weight PCs we compared them to the stimulus PCs. This significance criterion ensures that the semantic structure that we observe in the PCs is due primarily to the fMRI data and not the statistics of category co-occurrence in the stimuli.

We first tested whether each individual-subject model weight PC accounted for more variance than would be expected by chance. To find confidence intervals on the variance accounted for by each PC we bootstrapped the model weight PCA by sampling with replacement from the voxel population 1000 times. Similarly, confidence intervals on the variance in model weights accounted for by each stimulus PC were obtained by bootstrapping the stimulus PCA 1000 times. The amount of variance accounted for in the model weights by each of the model weight PCs (orange lines) and stimulus PCs (gray lines) is shown in Figure 3, along with error bars denoting 99% confidence intervals. To test the hypothesis that a model weight PC accounts for more variance than the corresponding stimulus PC we counted the number of times in the 1000 bootstrap samples that the stimulus PC accounted for more variance than the model weight PC. The null hypothesis for this analysis is that the stimulus PC and the model weight PC account for the same amount of variance. We rejected the null hypothesis if the stimulus PC never accounted for more variance than the voxel weight PC across the 1000 bootstrap samples (corresponding to $p < 0.001$).

Because lower-variance PCs are more sensitive to noise and thus more likely to yield false positives, we tested the PCs sequentially and stopped testing after encountering the first non-significant PC. This procedure revealed that subject SN has 6 significant PCs (which account for 29.6% of variance), AH has 7 significant PCs (which account for 33.1% of variance), AV has 7 significant PCs (which account for 35.5% of variance), TC has 7 significant PCs (which account for 34.3% of variance), and JG has 8 significant PCs (which account for 34.2% of variance).

Next we tested PCs constructed using combined data from many subjects. For each subject we constructed a set of group PCs using combined data from the other four subjects, leaving out the selected subject. For example, to test subject SN we performed PCA on combined model weights from subjects AH, AV, TC, and JG. We then computed the amount of variance accounted for in the model weights for the left out subject by each of the group PCs.

As with the individual subject PCs and stimulus PCs, confidence intervals on the variance explained by the group PCs were found using the bootstrap. We then tested whether each group PC explained more variance than the corresponding stimulus PC using the statistical procedure described above. We found that subjects SN, AH, AV, and TC were significantly explained by 4 group PCs (which accounted for 19.1%, 17.3%, 21.6%, and 20.6% of variance, respectively), and subject JG was significantly explained by 3 group PCs (which accounted for 15.4% of variance).

This analysis suggests that the five subjects share a common semantic space consisting of at least the first three group PCs, and four of the five subjects share four group PCs. We estimated the full group semantic space using PCA on combined data from all five subjects (49685 voxels total). The data were never spatially averaged across subjects, and never transformed into a standard functional brain space.

Supplemental References

- Aguirre, G. K., Zarahn, E., & D'Esposito, M. (1998). An Area within Human Ventral Cortex Sensitive to Building Stimuli: Evidence and Implications. *Neuron*, 21(2), 373-383.
- Avidan, Hasson, U., Malach, R., & Behrmann, M. (2005). Detailed exploration of face-related processing in congenital prosopagnosia: 2. Functional neuroimaging findings. *J Cogn Neurosci*, 17(7), 1150-1167.
- Brewer, A. a, Liu, J., Wade, A. R., & Wandell, B. a. (2005). Visual field maps and stimulus selectivity in human ventral occipital cortex. *Nat Neurosci*, 8(8), 1102-9. doi:10.1038/nn1507
- Corbetta, M., Akbudak, E., Conturo, T. E., Snyder, A. Z., Ollinger, J. M., Drury, H. A., Linenweber, M. R., et al. (1998). A common network of functional areas for attention and eye movements. *Neuron*, 21(4), 761-773.
- David, S. V., & Gallant, J. L. (2005). Predicting neuronal responses during natural vision. *Network: Computation in Neural Systems*, 16(2-3), 239-260.
- Downing, P. E., Jiang, Y., Shuman, M., & Kanwisher, N. (2001). A cortical area selective for visual processing of the human body. *Science*, 293(5539), 2470.
- Epstein, R., & Kanwisher, N. (1998). A cortical representation of the local visual environment. *Nature*, 392(6676), 598-601.
- Fried, I., Katz, A., McCarthy, G., Sass, K., Williamson, P., Spencer, S., & Spencer, D. (1991). Functional Organization of Human Supplementary Motor Cortex Studied by Electrical Stimulation Motor Cortex. *J Neurosci*, 11(November), 3656.
- Grosbras, M. H., Lobel, E., de Moortele, P. F. V., LeBihan, D., & Berthoz, A. (1999). An anatomical landmark for the supplementary eye fields in human revealed with functional magnetic resonance imaging. *Cereb Cortex*, 9(7), 705.
- Halgren, E., Dale, A. M., Sereno, M. I., Tootell, R. B. H., Marinkovic, K., & Rosen, B. R. (1999). Location of human face-selective cortex with respect to retinotopic areas. *Hum Brain Mapp*, 7(1), 29-37.
- Hansen, K. a, Kay, K. N., & Gallant, J. L. (2007). Topographic organization in and near human visual area V4. *J Neurosci*, 27(44), 11896-911. doi:10.1523/JNEUROSCI.2991-07.2007
- Hasson, U., Harel, M., Levy, I., & Malach, R. (2003). Large-scale mirror-symmetry organization of human occipito-temporal object areas. *Neuron*, 37(6), 1027-1041.
- Hoerl, A. E., & Kennard, R. W. (1970). Ridge Regression: Biased Estimation for Nonorthogonal Problems. *Technometrics*, 12(1), 55-67.
- Hsu, A., Borst, A., & Theunissen, F. (2004). Quantifying variability in neural responses and its application for the validation of model predictions. *Network: Computation in Neural Systems*, 15(2), 91-109. doi:10.1088/0954-898X/15/2/002
- Kanwisher, N., McDermott, J., & Chun, M. M. (1997). The fusiform face area: A module in human extrastriate cortex specialized for face perception. *J Neurosci*, 17(11), 4302-4311.
- McCarthy, Gregory, Puce, A., Gore, J. C., & Allison, T. (1997). Face-Specific Processing in the Human Fusiform Gyrus. *J Cogn Neurosci*, 9(5), 605-610. MIT Press. doi:10.1162/jocn.1997.9.5.605
- Nakamura, K., Kawashima, R., Sato, N., Nakamura, A., Sugiura, M., Kato, T., Hatano, K., et al. (2000). Functional delineation of the human occipito-temporal areas related to face and scene

processing. *Brain*, 123(9), 1903.

Paus, T. (1996). Location and function of the human frontal eye-field: a selective review. *Neuropsychologia*, 34(6), 475-483.

Peelen, M. V., & Downing, P. E. (2005). Selectivity for the human body in the fusiform gyrus. *J Neurophysiol*, 93(1), 603.

Penfield, W., & Boldrey, E. (1937). Somatic motor and sensory representation in the cerebral cortex of man as studied by electrical stimulation. *Brain*, 60(4), 389.

Rajimehr, R., Young, J. C., & Tootell, R. B. H. (2009). An anterior temporal face patch in human cortex, predicted by macaque maps. *Proc Natl Acad Sci U S A*, 106(6), 1995.

Sahani, M., & Linden, J. F. (2003). How linear are auditory cortical responses. *Advances in Neural Information Processing Systems*, 15, 109-116.

Schwarzlose, R., Baker, C., & Kanwisher, N. G. (2005). Separate face and body selectivity on the fusiform gyrus. *J Neurosci*, 25(47), 11055-11059.

Tootell, R. B., Reppas, J. B., Kwong, K. K., Malach, R., Born, R. T., Brady, T. J., Rosen, B. R., et al. (1995). Functional analysis of human MT and related visual cortical areas using magnetic resonance imaging. *J Neurosci*, 15(4), 3215.

Tsao, D. Y., Moeller, S., & Freiwald, W. A. (2008). Comparing face patch systems in macaques and humans. *Proc Natl Acad Sci U S A*, 105(49), 19514.